CSIRO PUBLISHING

Marine and Freshwater Research
http://dx.doi.org/10.1071/MF15043

Seasonal variability in turbidity currents in Lake Ohau, New Zealand, and their influence on sedimentation

R. Cossu[A,E], *A. L. Forrest*[A,B], *H. A. Roop*[C,D], *G. B. Dunbar*[D], *M. J. Vandergoes*[C], *R. H. Levy*[C], *P. Stumpner*[B] *and S. G. Schladow*[B]

[A]Australian Maritime College, University of Tasmania, Maritime Way, Newnham, Tas. 7248, Australia.
[B]Tahoe Environmental Research Center, Department of Civil and Environmental Engineering, University of California, 1 Shields Avenue, Davis, CA 95616, USA.
[C]GNS Science, Department of Paleontology, Fairway Drive, Avalon, 5010, New Zealand.
[D]Antarctic Research Centre, Victoria University of Wellington, Kelburn Parade, Wellington, 6140, New Zealand.
[E]Corresponding author. Email: remo.cossu@utas.edu.au

Abstract. Layers of sediment that are deposited on the floor of Lake Ohau, New Zealand, offer a means to reconstruct past climate conditions in the Southern Hemisphere at subdecadal and annual resolution. A robust understanding of the modern physical processes that control the influx and dispersal of sediment in the lake is required to reconstruct climate from these sedimentary archives. In this study, water temperature and velocity measurements collected during 2012–13 were analysed to determine the primary physical processes that influence sediment transport in the lake. Sediment input from river inflow occurs throughout the year but exhibits strong seasonal variation. Large inflow events ($Q > 500\ m^3\ s^{-1}$) that follow strong summer rainstorms trigger high-concentration turbidity currents, which are the main agents for sediment delivery and deposition. During winter, smaller turbidity currents also occur after rain events and contribute to annual sediment accumulation. In addition, large internal waves were observed during the summer and may influence sedimentation. In conclusion, several processes including river inflow, internal waves and convectively driven flows control sediment deposition and accumulation in the Lake Ohau system. We utilise these observations to establish a conceptual model to explain the observed infill stratigraphy in Lake Ohau and guide interpretation of the longer sedimentary record.

Received 3 February 2015, accepted 7 August 2015, published online 4 November 2015

Introduction

Sedimentation patterns in alpine and temperate lakes can be strongly influenced by the magnitude and physical properties of river inflows (Hamblin and Carmack 1978; Alavian *et al.* 1992; De Cesare *et al.* 2006). In particular, increased river inflow in response to rainfall and the spring freshet can form gravity currents carrying large sediment loads into lakes (Weirich 1986; Desloges and Gilbert 1994; Gilbert *et al.* 2006; Amann *et al.* 2014). Seasonal variability in river-fed lakes can influence sedimentation and produce clastic varves, e.g. relatively thick layers of coarse sediment during summer and thinner layers of fine sediments during winter (e.g. Leemann and Niessen 1994; Gilbert and Butler 2004). In order to use clastic varves to reconstruct past climate, establishing the linkages between meteorological, limnological and sedimentary processes in lakes is required (e.g. Leemann and Niessen 1994; Hardy 1996). Lake-monitoring programs provide measurements of physical properties in the water column (e.g. temperature, river inflow, velocities) and sediment characteristics (e.g. turbidity, particle concentration, particle size) that can help identify the control processes on sedimentation and to accurately interpret the sedimentary record preserved in the lake bed (Leemann and Niessen 1994; Tylmann *et al.* 2012; Ojala *et al.* 2012).

Many lake systems and their associated sedimentation regimes have been studied in the Northern Hemisphere (e.g. Pharo and Carmack 1979; Mulder and Syvitski 1995; Gilbert and Crookshanks 2009) and have been used to generate annually resolved palaeoclimate reconstructions (e.g. Gilbert 1975; Desloges 1994; Leemann and Niessen 1994; Hardy 1996; Gilbert *et al.* 2006; Amann *et al.* 2014; and many others). Similar studies are largely absent from the Southern Hemisphere (Ojala *et al.* 2012) despite the potential to gain insight into Pacific and Southern Hemisphere climate modes including El Niño–Southern Oscillation and the Southern Annular Mode, which regulates the Southern Hemisphere westerly winds (Thompson and Solomon 2002; Ummenhofer *et al.* 2009).

Located on the South Island of New Zealand, Lake Ohau offers a prime target to address this gap in global climate records as it sits near the northern boundary of the westerly winds that dominate atmospheric circulation. A 70-m-thick sequence of

sediments in the lake basin offers the potential to examine climate evolution in the Southern Hemisphere since the end of the last glacial maximum (*c.* 17 000 years ago). Fine-scale (mm) laminations preserved in lake floor sediment likely form in response to seasonal variability in hydroclimate (Roop *et al.* 2015). However, detailed examination of hydrodynamic conditions through the seasonal variations is required to improve our understanding of sediment dispersal within the lake and identify the cause(s) of millimetre-scale varves.

In this paper we examine temperature, current velocity, and turbidity data acquired near the dominant inflow of Lake Ohau to explore the effect of changing physical properties in the water column on sedimentation over an annual cycle. Constraining the role of large flood events is a particular focus as heavy rainstorms can trigger sedimentation rates on the order of 15 mm year^{-1} at the distal end of the lake and >200 mm year^{-1} near the river delta (Roop *et al.* 2015). Clearly, flood-related large turbidity currents, internal waves and convectively driven density currents have an effect on long-term sedimentation patterns in the Lake Ohau system. The development of a conceptual model that integrates these elements is a primary aim of this research.

Material and methods

Site description

Lake Ohau (44°14.040′S, 169°51.240′E; 520 m above sea level) is one of three north–south trending lakes formed during the rapid glacial retreat between 17 900 and 17 4000 years ago following the last glacial maximum on the South Island of New Zealand (Fig. 1*b*) (Putnam *et al.* 2013). The lake lies in the intermontane Mackenzie Basin, is 18.5 km long, up to 5 km wide

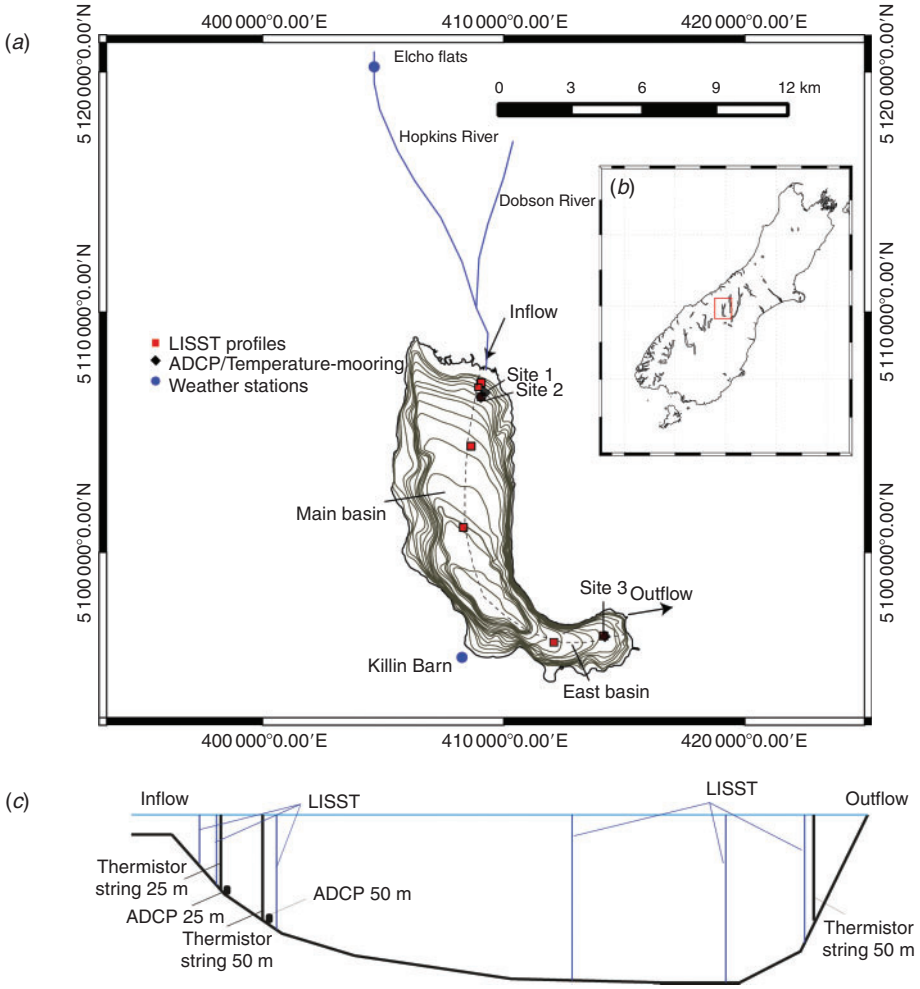

Fig. 1. (*a*) Map of Lake Ohau and locations of the moorings, LISST profiles and weather stations. The dashed line depicts the longitudinal profile shown in (*c*); (*b*) location of Lake Ohau in South Island, New Zealand; and (*c*) longitudinal profile of Lake Ohau (vertical exaggeration) with position of instruments. Two thermistor chains were arranged in depths of 25 m and 50 m near the head of the lake (Sites 1 and 2) and one thermistor chain near the outflow in the south-east (Site 3). Two ADCPs were located next to the moorings near the inflow at similar depths of 25 m and 50 m (Sites 1 and 2). LISST profiles were taken along the lake axis as shown in (*a*).

with a total surface area of ~54 km^2. The lake has a mean depth of 74 m but reaches a maximum depth of 129 m along its central axis. Important bathymetric features are the steep delta front near the head of the lake where the depth increases rapidly to >100 m (with a slope of ~5%) and a sharp 90° turn to the east located in the southern portion of the lake, which separates the main basin and the eastern end of the lake (Fig. 1).

Water inflow into the lake is mainly controlled by the Hopkins and Dobson Rivers, which drain a combined area of 924 km^2 before converging just upstream of the lake and contributing ~85% of the total annual inflow (Woods *et al.* 2006). The inflow rates into Lake Ohau predominantly depend on summer precipitation and summer snowmelt (17% of total annual flow: Kerr 2013) with an increase in discharge during the spring freshet (October–November) and typically lower inflow rates during the winter period (Roop *et al.* 2015, and references therein).

Instrument deployment and data acquisition

Two arrays of instruments were deployed between January 2012 and January 2013 near the head of the lake at 25-m water depth (44°11.069′S, 169°51.680′E) and at 50-m water depth (44°11.368′S, 169°51.718′E). Each of the two moorings consisted of one thermistor chain and one Teledyne Acoustic Doppler Current Profiler (ADCP; Teledyne, Los Angeles, CA, USA) (Fig. 1). The thermistor chains had seven individual temperature loggers (TR-1060, RBR, Kanata, ON, Canada), which were located at 5-, 10-, 20-, 25-, 30-, 35- and 45-m water depth. The loggers had an accuracy of 0.002°C (resolution of <0.00005°C) and a sampling interval of 5 s. All loggers were calibrated and synchronised before the start of the instrument deployment. Additional temperature information was recorded using Onset HOBO Water Temperature Pro v2 data loggers (Bourne, MA, USA) with an accuracy of 0.2°C (resolution of 0.02°C). Temperature data with the HOBO loggers were collected at 5-min intervals at 2.5-, 7.5-, 13-, 17-, 22-, 27.5-, 32.5-, 37.5- and 42.5-m water depth. An additional Onset HOBO thermistor chain was located near the outflow (44°16.782′S, 169°55.480′E) with loggers at 5, 21, 36 and 51 m water depth, which recorded at 5-min intervals (positions of all instrumentation shown in Fig. 1*c*).

Density was computed using the linear freshwater equation of state (Chen and Millero 1986). The position, h, of the height of the seasonal thermocline above the lakebed was established by determining the location of maximum density gradient by using the first moment of the density gradient (Patterson *et al.* 1984):

$$h = \int_0^H z\frac{\partial\rho}{\partial z}dz \Big/ \int_0^H \frac{\partial\rho}{\partial z}dz \qquad (1)$$

where ρ is the density of water (kg m^{-3}), H is the entire thickness of the water column (m) and z is the depth measured from the surface (m).

Velocity data were collected using a RDI 1200-kHz, 4-beam ADCP moored on the bottom near the thermistor chain at a depth of 25 m and a RDI 600-kHz, 4-beam ADCP at depth of 50 m (Fig. 1). The ADCP recorded velocities of the four beams (Mode 1) every 30 min in bins of 1 m starting from 1 m above the lake bottom. For both instruments, the resolution and accuracy were 0.001 and ±0.0003 m s^{-1} respectively. A total of 240 pings were averaged per sample. Horizontal velocity data were calculated using

$$v_{hor} = \sqrt{v_{east}^2 + v_{north}^2}$$

where v_{east} and v_{north} are the directional velocity components. ADCP data were available only until early January 2013 as both ADCPs were covered with sediment, and one was lost completely, during a large flood event.

River inflow data are estimated using a mass balance approach using a combination of measured outflow and lake level records collected by Meridian Energy Ltd. Weather data, including temperature (HP35C Campbell Scientific, Logan, UT, USA), solar radiation (Li-200 pyranometer Li-Cor, Lincoln, NB, USA) and wind speed and direction (3002 RM Young, Traverse City, MI, USA; 3-m height), were obtained at 10-min intervals from the automated Killin Barn weather station located south-west of the lake (44°11.274′S, 169°51.841′E) and precipitation data were collected at the Elcho Flats station (43°11.924′S, 169°51.838′E) (managed by Meridian Energy Ltd), upstream of Lake Ohau (both sites labelled in Fig. 1). Using these meteorological data along with the measured surface water temperatures, the four main heat flux components, net shortwave irradiance (SW), net longwave radiation (LW, determined after the Tennessee Valley Authority; Wunderlich 1972), sensible heat (H), and latent heat (kE) can be used to estimate net heat flux using a similar approach and assumptions as detailed in Forrest *et al.* (2008).

An additional dataset of suspended sediment concentration and particle size distribution was measured in June 2012 with a Laser *In Situ* Scattering and Transmissometry 100X Type B instrument (LISST-100X) from Sequoia Scientific, Inc (Bellevue, WA, USA). The LISST-100X was used to take vertical profiles at six different locations along the thalweg of the lake (see Fig. 1*a*, *c*) during a winter flood event at DOY (day of year) 175. The sampling rate was 1 Hz and the particle size range detectable with the instrument is 1.25–250 µm.

Results

Annual meteorological cycle

Fig. 2 summarises the meteorological observations made during the on-site measurements. Air temperature records reveal large seasonal and diurnal variability (Fig. 2*a*), consistent with the intermontane setting. Precipitation at the Elcho Flats Station shows strong rain events throughout the year (Fig. 2*b*). Average wind speeds are generally smaller in autumn and winter (Fig. 2*c*). However, strong wind events (>8.0 m s^{-1}) prevail throughout the entire year (Fig. 2*c*) and consistently originate from the north-north-east as down-valley winds. During winter, the average river discharge (Q_{av}) is ~60 m^3 s^{-1}, with several flood events exceeding 200 m^3 s^{-1} (Fig. 2*d*). There is an increase in the average discharge Q_{av} to 105 m^3 s^{-1} during summer, with two peak discharge events (Q ~ 1000 m^3 s^{-1}) on 4 and 10 January 2013. Generally, these discharge measurements

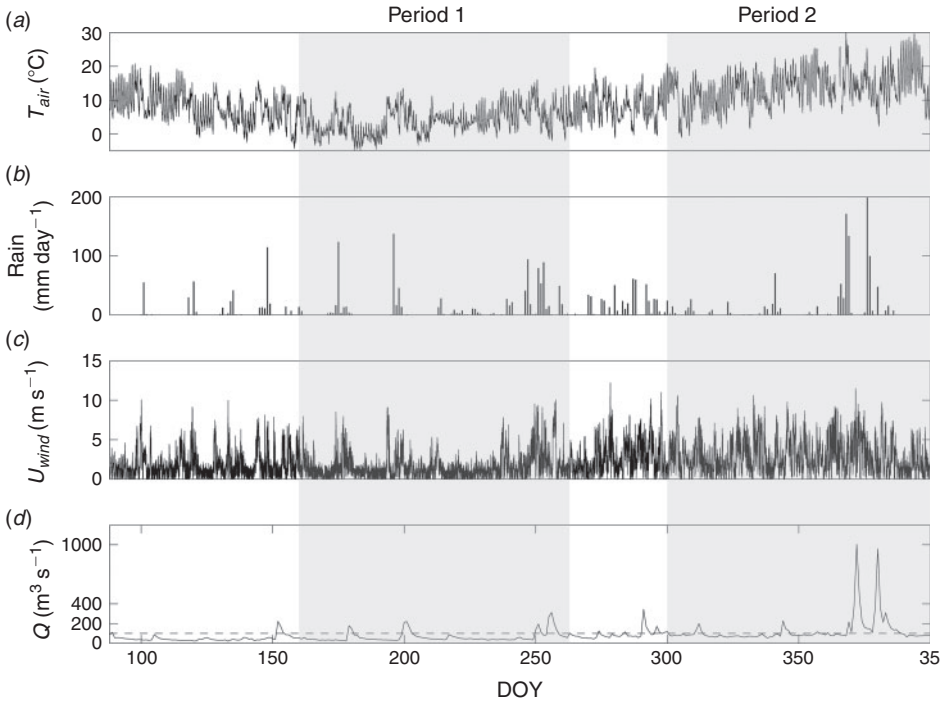

Fig. 2. Recorded weather data for Lake Ohau during the experiment. (*a*) Air temperature measured at Killin Barn; (*b*) precipitation measured at Elcho Flats station upstream of Lake Ohau; (*c*) observed wind velocity for Killin Barn; and (*d*) estimated inflow (Q) into Lake Ohau during the experiment. Dashed line represents a discharge of $Q = 100$ m^3 s^{-1}.

are congruent with records dating back to 1926, with flow peaks in December or January. However, large flood events of the magnitude recorded in January 2013 have occurred fewer than 10 times since the beginning of the historical record in 1926 (Roop *et al.* 2015). In this paper we distinguish between average discharge for $Q < 100$ m^3 s^{-1}, flood events with $Q > 100$ m^3 s^{-1} (occurring several times per year, marked by dashed line in Fig. 2*d*) and large flood events, which have $Q > 500$ m^3 s^{-1} (with a return period of >2 years). As shown in all panels of Fig. 2, weather data correlate well with estimates of river inflow as peak inflow rates directly follow episodic storm events and associated periods of rain.

As highlighted in Fig. 2 with the grey bars, we focus on two significant thermal regimes occurring in winter (Period 1), associated with a weakly stratified water column, and in summer (Period 2), associated with a stratified water column. These two periods, as defined in Roop *et al.* (2015), are hypothesised to significantly contribute to intra-annual variations in lake floor stratigraphy.

Winter period (Period 1: DOY 160–260)

Fig. 3 shows the weather data, temperature and velocities in the water column at Site 2 during Period 1 (DOY 160–260). Air temperatures reveal a diurnal variability with a mean temperature of ~4°C (Fig. 3*a*). There are several rain events where precipitation exceeds 10 mm day^{-1} (Fig. 3*b*) followed by significant flooding (Fig. 3*c*). The most prominent flood event was observed between DOY 195 and DOY 200, when inflow rates peaked at values of $Q = 250$ m^3 s^{-1}. Predominantly calm or light winds prevail with a mean wind speed, $U_{wind} = 3$ m s^{-1}. This value was exceeded on only three occasions when wind speeds were >5 m s^{-1} (Fig. 3*d*).

The temperature in the water column was ~10°C on DOY 160 and dropped down to minimum values of 7–8°C by DOY 240 (Fig. 3*e*). Temperature variability was very small throughout the water column, with the largest differences occurring near the bottom. In particular, periodic temperature variations of 1–2°C were present within 5 m off the lakebed between DOY 200 and 250 (delimited by the black dashed arrow). Horizontal velocities in the water column are illustrated in Fig. 3*f*. Close to the bottom, the horizontal velocities were observed to fluctuate between 0.02 and 0.1 m s^{-1}, with episodic increases of up to 0.25–0.3 m s^{-1} when river inflow rates are large (e.g. on DOY 195 to DOY 200 and DOY 214 to DOY 216). Although not shown, periods of large velocities have a flow direction consistently towards south and south-east. In contrast, small velocity fluctuations of 0.02–0.05 m s^{-1} during periods of low inflow correlate well with small periodic temperature variations near the bottom (e.g. between DOY 200 and DOY 230). The recorded Echo intensity (EI) of the four ADCP beams at 5 m above the bed is shown in Fig. 3*h* and has a mean value of EI ~ 100 dB (horizontal line) during Period 1. We interpret this EI count as a relative estimate of acoustic backscatter, inferring an increased sediment load being present in the water column (Kim and Voulgaris 2003). Significant increases of up to EI = 170 dB

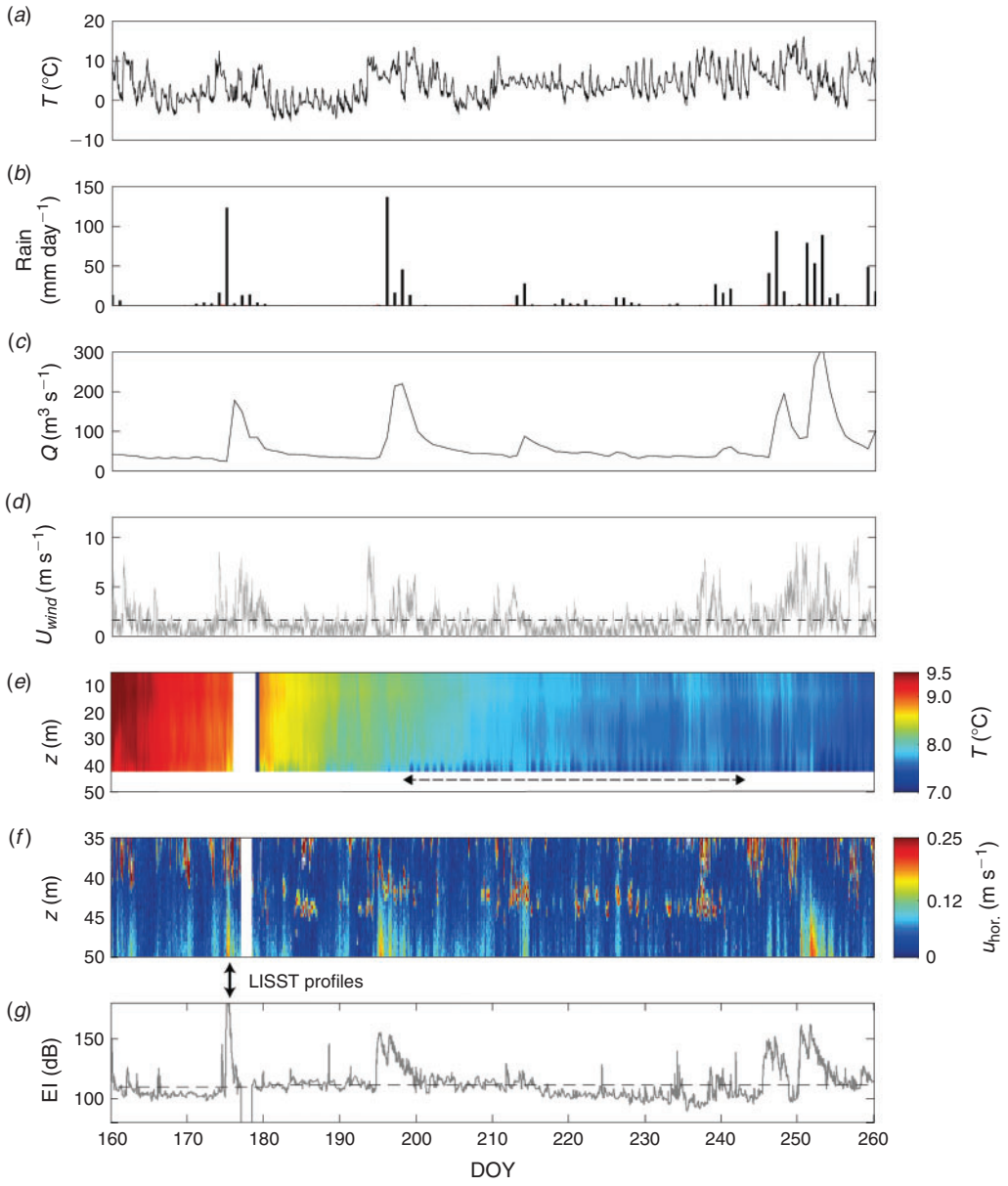

Fig. 3. Observed weather and limnological parameters in the water column during Period 1. (*a*) Recorded temperature at Killin Barn; (*b*) measured rainfall at Elcho Flats; (*c*) estimated inflow for Lake Ohau; (*d*) observed wind speed at Killin Barn (mean wind speed is marked by the dashed line); (*e*) temperature observed at the 50-m mooring near the inflow (the horizontal arrow indicates the time when periodic temperature fluctuations near the bottom were observed); (*f*) horizontal ADCP velocities at the 50-m mooring; and (*g*) ADCP echo intensities (EI) measured 5 m above the bottom. The average EI is shown by the dashed black line.

occurred during periods from DOY 175 to 178, DOY 195 to 200 and DOY 245 to 255, which correlates well with periods of increased river inflows, larger horizontal and vertical velocities respectively.

Fig. 4 shows the measured sediment concentration profiles at six locations (see Fig. 1*a*) collected during an inflow event with $Q > 180$ m^3 s^{-1} at DOY 175 (marked by arrow in Fig. 3). This inflow was characterised by maximum velocities of 0.2 m s^{-1} and EI values of 180 dB. At most locations, the largest concentrations (μL L^{-1}) were close to the lakebed and Fig. 4*c–f* exhibits typical underflow profiles similar to the observed velocity distribution in Period 1. Interestingly, the distribution of particles in the deepest part in the lake (Fig. 4*e*) has highest concentrations between $z = 80$ and $z = 100$ m. Nonetheless, near the outflow, the water column reveals the highest concentrations in the lake with a typical nose-shaped profile of an underflow (Middleton 1993). This sediment underflow is attributed to accumulation of sediments between $z = 50$ and 60 m after the flow has passed through the deepest part of the lake (Fig. 4*e*) and runs into the eastern basin with shallower

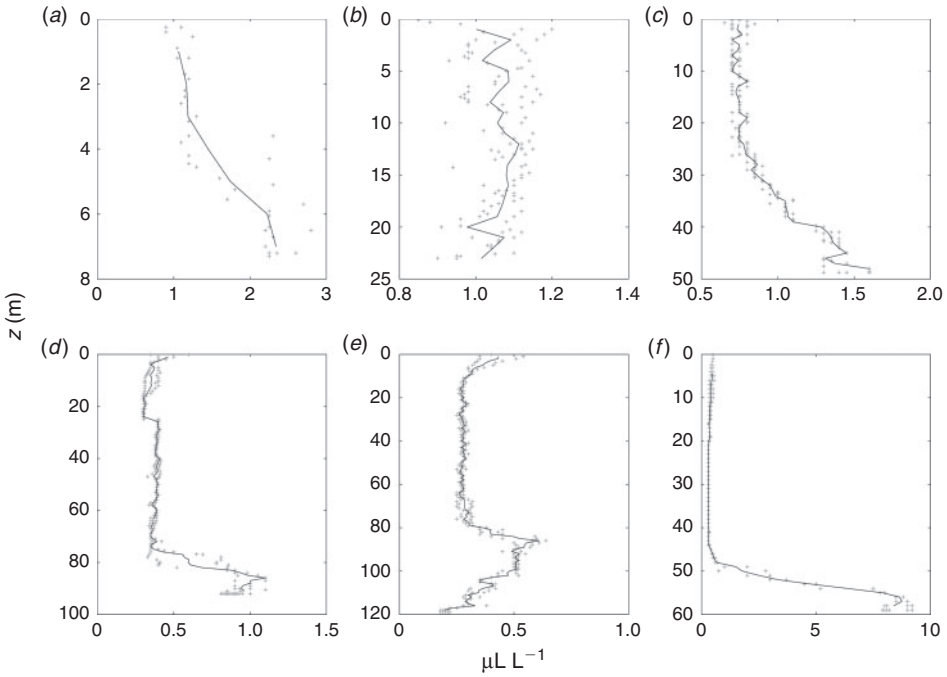

Fig. 4. Vertical sediment concentration profiles (LISST) measured at DOY 175 2012 between 1100 and 1300 hours in Lake Ohau. Panels (*a*) to (*f*) depict the sediment particle distribution (μL L^{-1}) at locations shown in Fig. 1*c*. Solid lines represent averaged values of 1-m bins.

bathymetry. It is proposed that this event typifies underflow conditions during Period 1 (see Discussion).

Spring–summer period (Period 2: DOY 300 in 2012 to DOY 35 in 2013)

Fig. 5 depicts the weather data and corresponding processes in the water column at Site 2 between DOY 300 in 2012 and DOY 35 in 2013. Air temperatures reveal a large seasonal and diurnal variability but also a constant increase of temperatures from 8°C to 14°C (Fig. 5*a*). There are several large rain events (>20 mm day^{-1}: Fig. 5*b*), which correlate well with inflow rates shown in Fig. 5*c*. The average discharge rates remain fairly constant ($Q \sim 80$ m^3 s^{-1}) but show episodic, rapid increases of up to $Q = 150$–200 m^3 s^{-1} lasting for several days (Fig. 5*c*). The two most significant events occurred between DOY 3 and 7 and DOY 10 and 15 in 2013 when inflow rates peaked at 1000 m^3 s^{-1} and were associated with heavy rain events. Wind data strongly fluctuate, with the mean wind speed being 4 m s^{-1} and peak wind speeds exceeding 8 m s^{-1} on numerous occasions (Fig. 5*d*).

During Period 2, epilimnetic water temperatures range from 8°C to ~14°C in the bottom waters (Fig. 5*e*). The epilimnion deepens continuously from an average depth of 20 m at DOY 320 to 30 m at DOY 35 in 2013. The thermocline shows strong excursions with a maximum depth at 35 m (DOY 10, 2013) and a minimum depth of 3 m (DOY 3, 2013). Horizontal velocities show episodic, large increases near the bottom with peak velocities of up to 0.4 m s^{-1} (DOY 10, 2013). These increased velocities are in close agreement with increased river inflow rates into the lake (Fig. 5*c*, *g*) and have flow direction towards south and south-east similar to Period 1. The averaged EI taken 5 m above the bottom, which ranges from EI = 100 dB to EI = 200 dB, is shown in Fig. 5*g*. In the same way that EI was interpreted for Period 1, the intensity peaks correlate well with increased horizontal and vertical velocities near the bottom, and are suggestive of high sediment transport during times of large inflows into the lake.

Discussion

For a climate-proxy site it is crucial to understand the significance of processes prevalent in the lake influencing deposition. The data from 2012–13 suggest a complex interaction of several limnological factors, such as sediment-laden density currents, internal wave action and convectively driven currents.

Turbidity density currents

Fig. 6*a* shows the vertical velocity profile of a turbidity current obtained by averaging a 3-h period of quasisteady flow conditions during an inflow event of $Q > 300$ m^3 s^{-1} at DOY 250. At the 25-m mooring (closed circles), maximum horizontal velocities reach 0.2 m s^{-1} near the bottom, which decrease to <0.05 m s^{-1} at 5 m above the bottom. The vertical velocity profile in Fig. 6*b* displays a similar shape with maximum downward-directed velocities of 0.02 m s^{-1} near the bed, which then reach background velocities by a height of 5–6 m above the bottom. Additionally, EI reduces from its maximum value of 200 dB near the lakebed to less than 50 dB at 8 m above the bed (Fig. 6*c*).

The same underflow was monitored at the 50-m mooring (open circles) where maximum horizontal flow velocities reached 0.25 m s^{-1} near the bed, which reduce to less than

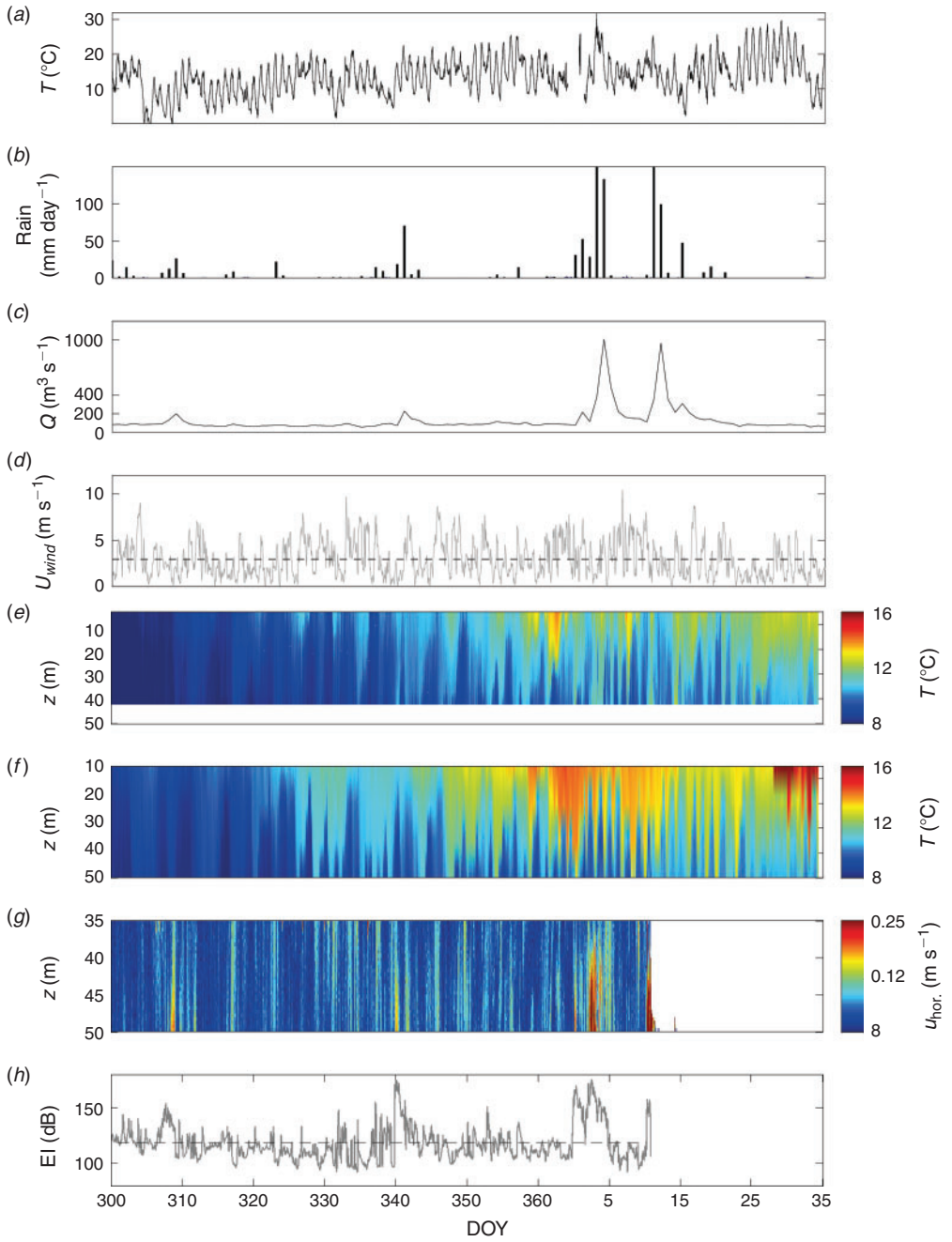

Fig. 5. Observed weather and parameters in the water column during Period 2. (*a*) Recorded temperature at Killin Barn; (*b*) measured rainfall at Elcho Flats; (*c*) estimated inflow for Lake Ohau; (*d*) observed wind speed at Killin Barn (mean wind speed is marked by the dashed line); (*e*) temperature observed at the 50-m mooring near the inflow (Site 2); (*f*) temperature observed at the 50-m mooring near the outflow (Site 3); (*g*) horizontal ADCP velocities at the 50-m mooring; and (*h*) ADCP echo intensities (EI) measured 5 m above the bottom (the average EI is shown by the dashed black line).

0.05 m s^{-1} at 15 m above the bottom (Fig. 6*d*). In contrast, vertical velocities showed no significant change, indicating that the flow was almost horizontal by this stage (Fig. 6*b*). EI values in Fig. 6*c* revealed an identical profile with maximum intensities near the bed (EI = 160 dB) and significantly lower intensities (EI = 50 dB) at 20 m above the bed. Thus, a turbidity current with a height of approximately $h = 5$–10 m passed Site 1 over a period of 3 h. Owing to entrainment of ambient fluid the height of the current increased to $h = 20$ m and passed Site 2. Furthermore, the reduced EI near the bottom suggests that sediment particle concentration decreased due to entrainment of ambient water along the slope (e.g. Best *et al.* 2005, and references

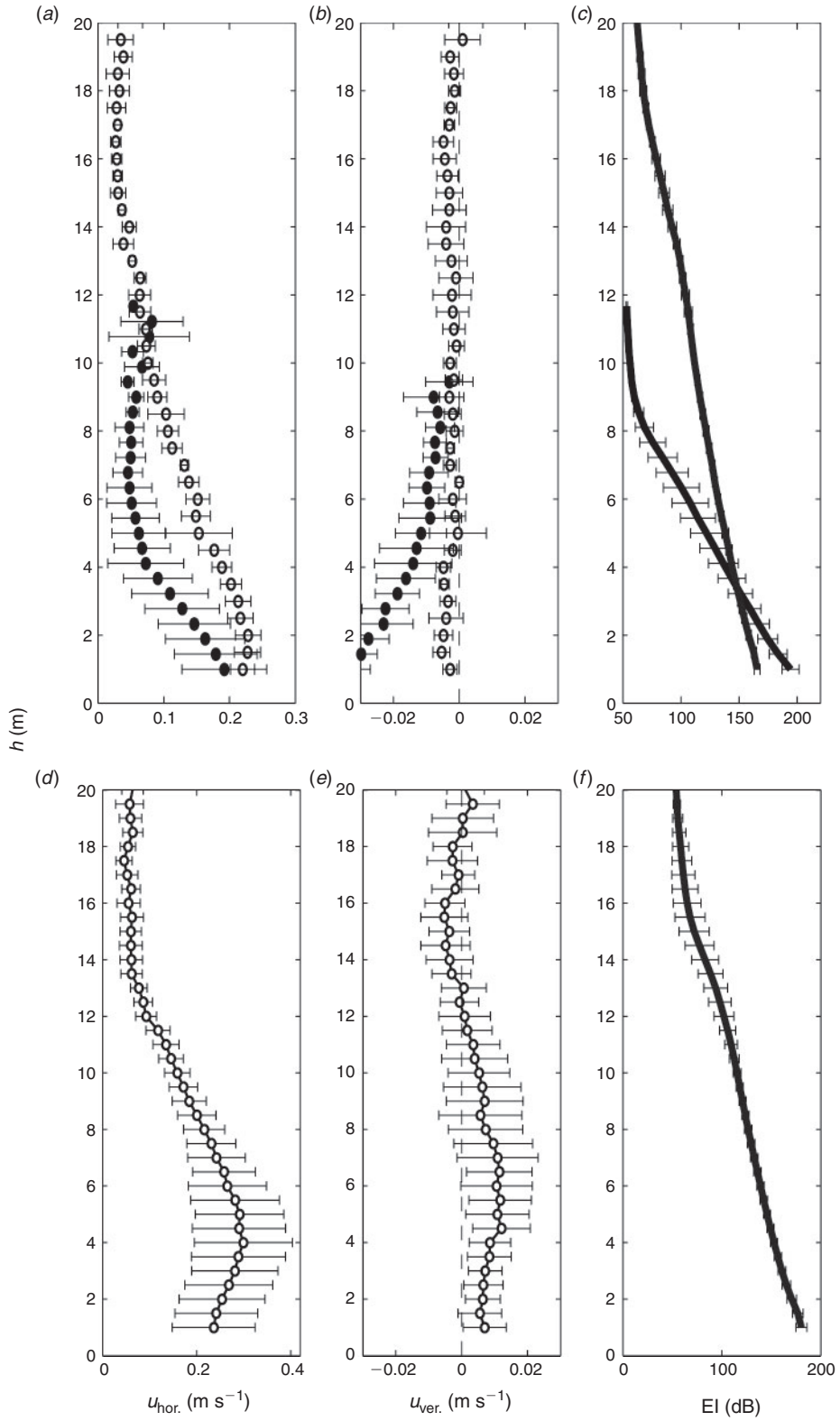

Fig. 6. Vertical profiles of observed turbidity currents near the inflow. (*a*) Horizontal velocity; and (*b*) vertical velocities during a flood event at DOY 250 in Period 1 (solid circles reflect measurements at the 25-m site and open circles reflect data from the 50-m site); (*c*) EI during the same event (black curve refers to the 25-m site and the grey curve to the 50-m site); (*d*) horizontal velocity; and (*e*) vertical velocity profile during the large flood event in Period 2 at the 50-m site; and (*f*) observed EI during this event (error bars in panels indicate standard deviation of the measured data during a 3-h period).

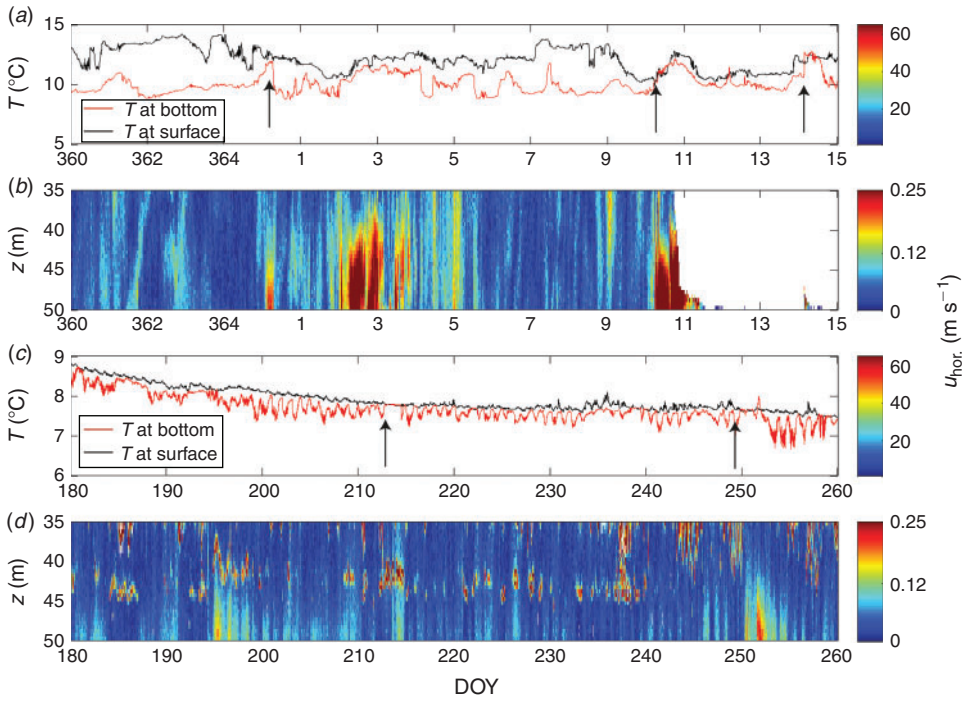

Fig. 7. Close-up of temperatures and velocities in the water column during turbidity currents. (*a*) Temperatures of the top thermistor ($z = 5$ m, black) and the bottom thermistor ($z = 42.5$ m, red); (*b*) horizontal velocities in the water column at the 50-m site; (*c*) temperatures of the top thermistor ($z = 5$ m, black) and the bottom thermistor ($z = 42.5$ m, red) in Period 1; and (*d*) horizontal velocities in the water column at the 50-m site in Period 1 (the arrows indicate the onset of temperature inversions, when water temperatures at the bottom were warmer than at the top).

therein). A simple one-dimensional approximation where the entrainment is approximated by $E \sim dh/dx$, with x being 1 km between the two sites, yields $E = 0.005$–0.015, which is found in many laboratory and field studies (Baringer and Price 1997; Dallimore *et al.* 2001; Cenedese *et al.* 2004), summarised in Wells *et al.* (2010).

The first large flood event during the summer at DOY 1–3 in 2013 is shown in Fig. 6*d–f*. Data were averaged over a 3-h period of quasisteady flow conditions at Site 2 and there were no ADCP data available from Site 1. The velocities show the typical nose-shaped profile of turbidity currents (e.g. Middleton 1993), with velocities of up to 0.25 m s^{-1} near the bed, before reaching the maximum velocities of 0.3 m s^{-1} at $z = 4$ m, which eventually reduce to 0.05 m s^{-1} at 15 m above the bottom (Fig. 6*d*). Vertical velocities reveal a constant upward direction of flow of 0.01 m s^{-1} between the bottom and a height of $z = 15$ m (Fig. 6*e*). Additionally, the EI profile has a maximum near the bottom (200 dB) and continuously decreases to 80 dB at $z = \sim 20$ m (Fig. 6*f*).

We found similar velocity and EI profiles seven times (not shown here) during increased river inflow providing irrevocable evidence of turbidity currents being generated near the bottom (50 m) by river discharges in Lake Ohau. Moreover, increased EI values support the hypothesis that turbidity currents can be associated with increased sediment transport and that they occur mainly near the bottom of Lake Ohau at the measuring sites.

Fig. 7*a* shows the recorded temperature measured 5 m below the surface and 5 m above the lake bed during the large floods (DOY 360 2012 to DOY 15 2013), and Fig. 7*b* depicts corresponding horizontal velocities within the bottom 15 m. Interestingly, at DOY 365, DOY 1–3, DOY 11 and DOY 14 bottom temperatures increase rapidly by up to 2°C, indicating that warmer water is descending down the slope. During two events of increased velocities near the lake bed (on DOY 1–4 and DOY 10–11) temperatures were observed to be greater near the lakebed than at the surface (Fig. 7*a*). Velocities and height of the gravity current are of the same order of magnitude as an inflow event observed in Lillooet Lake (Best *et al.* 2005). Temperature inversions over such a large depth range are possible only if the underflow had a large sediment concentration to overcome the buoyancy arising from the warmer water when it is dragged downslope by the current. For instance, De Cesare *et al.* (2006) found warm density currents piercing through the 20-m thermocline and intruding down to a depth of >200 m in Lake Lugano owing to high sediment concentrations. Similar riverborne turbidity currents with temperature anomalies of up to 3.5°C were reported in Lambert and Giovanoli (1988) where warm temperatures indicated that river water moved as an underflow through Lake Geneva due to short-term increases in sediment concentration.

Additional temperature anomalies between the top and the bottom waters were also observed in the winter (Fig. 7*c*). Sudden increases of horizontal velocities (Fig. 7*d*) correlate

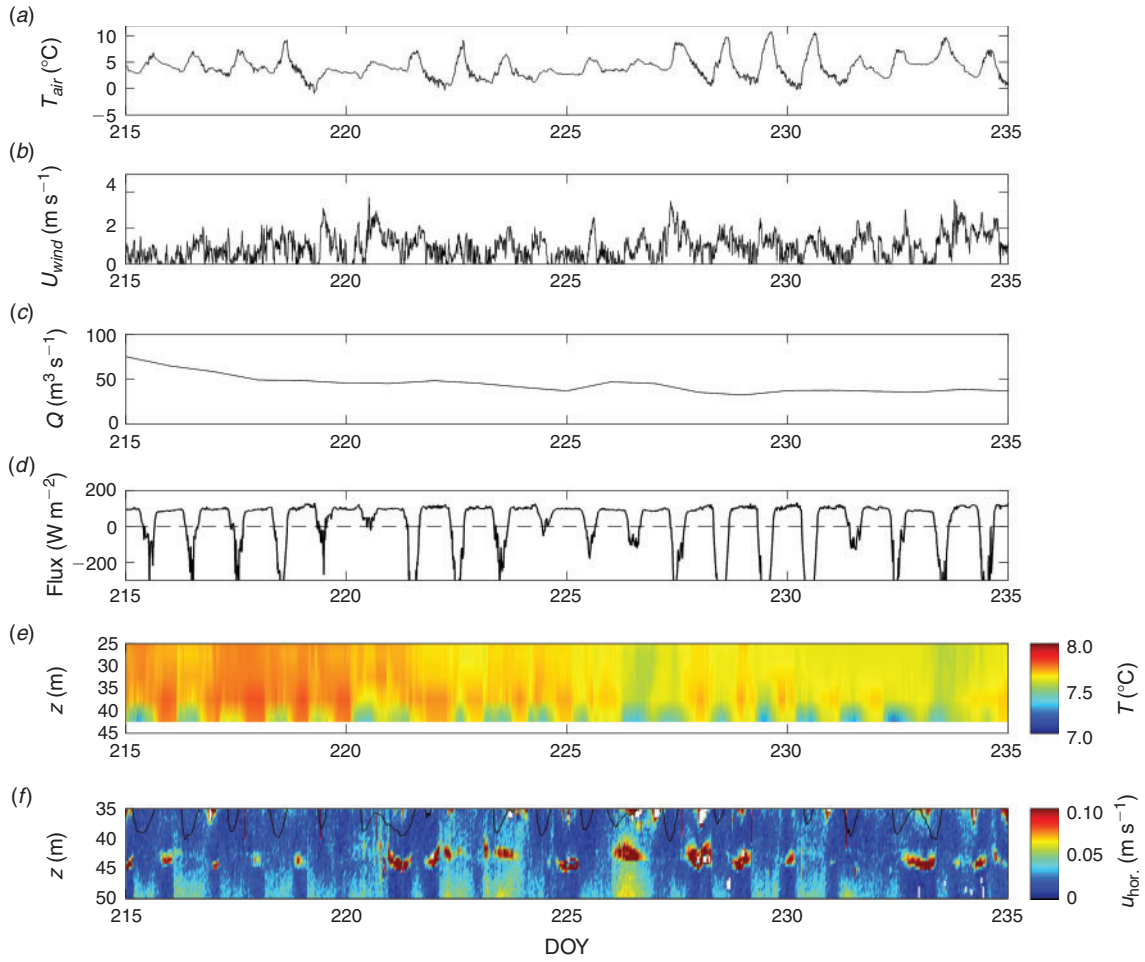

Fig. 8. Meteorological and limnological observations made between DOY 215 and DOY 235 in Period 1. (*a*) Air temperature; (*b*) wind speed; (*c*) inflow into Lake Ohau; (*d*) estimated net heat flux (positive values represent heat gained by the lake); (*e*) temperature observed at the 50-m mooring near the inflow; and (*f*) horizontal ADCP velocities at the 50-m mooring.

well with these inversions and are again attributed to turbidity currents that descend along the lakebed. Compared with summer inflow events the temperatures rise only by 0.5°C owing to nearly isothermal conditions. Nonetheless, the density difference required to overcome the buoyancy of warm water plunging down a slope with colder ambient water can only stem from suspended sediment particles in turbidity currents. Thus, these flows in Period 1 underline the importance of turbidity currents as an agent for sediment transport in the lake during winter.

Convection currents

Recall how Fig. 3 shows diurnal changes in water temperature and velocity near the bottom suggestive of the presence of another forcing mechanism, other than increased river inflow, during the destratified Period 1. The temperature in shallow, well mixed waters at the edges of lakes can cool more rapidly than that of adjacent deeper waters, in particular during periods of winter cooling. The resulting differential heating between the pelagic and littoral waters have been found to form cold, dense gravity currents along lake boundaries from shallow to deeper parts. For instance, cold-water plumes with a thickness of 10 m adjacent to the lake boundary were generated in the near-surface convective mixed layer when air temperatures were 7°C below the surface water temperature (Thorpe *et al.* 1999). Similar observations have been reported in other lakes (Fer *et al.* 2002; Jonas *et al.* 2003; Forrest *et al.* 2008). Consistent in these studies was a net heat flux, which demonstrated cooling during the night (heat loss) so that dense cold-water plumes eroded the stratification that had developed during daytime.

Fig. 8 compares air temperature (Fig. 8*a*), wind speed (Fig. 8*b*), inflow rates (Fig. 8*c*), the estimated heat flux (Fig. 8*d*) as well as the observed temperature (Fig. 8*e*) and horizontal velocities (Fig. 8*f*) in the water column at Site 2 between DOY 215 to DOY 235. Periodic temperature fluctuations of ~1°C and velocities near the bottom up to 0.1 m s^{-1} correspond to air temperature changes but they do not correlate well with the low, constant inflow rates ($Q < 60$ m^3 s^{-1}) or low wind speeds (<3 m s^{-1}). In contrast, the estimated heat flux of 150 W m^{-2} from the lake to the atmosphere is of the same order of magnitude as has been documented in other lakes (e.g. Jonas *et al.* 2003; Forrest *et al.* 2008) where sufficient heat loss at night drives the formation of cold density plumes. Furthermore, the

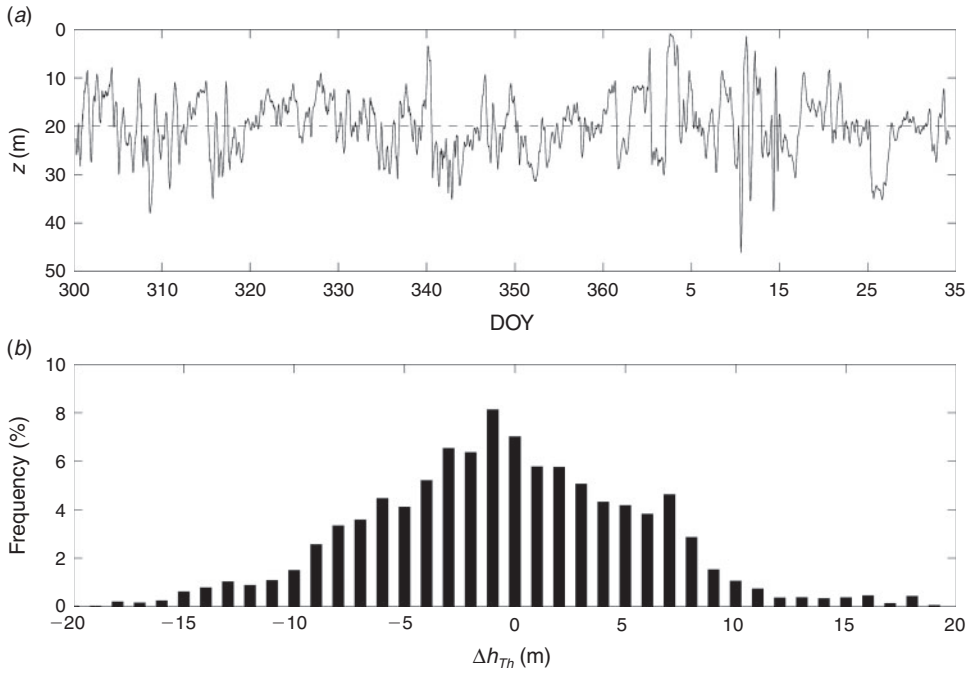

Fig. 9. Frequency distributions of thermocline excursions at the 50-m mooring near the inflow. (*a*) Calculated height of the thermocline (the mean depth is shown by the dashed line); and (*b*) frequency distribution of the magnitude of the thermocline excursion (Δz_{Th}).

constant periodicity of ~24-h period supports the idea that downslope flows of cold dense water plumes occur at the head of the lake in response to diurnal heating and cooling.

Internal waves

One of the major controls on hydrodynamics in temperate lakes is the density stratification of the water column due to solar heating in the summer. Fig. 5 compares the inflow rates (Fig. 5*a*), wind velocities (Fig. 5*b*) and the thermal variability near the inflow (Fig. 5*e*) and outflow (Fig. 5*f*) for Period 2. Lake Ohau starts to stratify after DOY 320 when a strong temperature gradient (thermocline) develops. The thermal regime reveals up to 4°C colder temperatures near the inflow compared with the outflow, which can most likely be attributed to cold river inflow.

The mean depth of the thermocline near the inflow is approximately $z_{Th} = 20$ m but the depth varies greatly, as demonstrated by excursions close to the water surface and bottom during peak inflow (DOY 3 or DOY 10 in 2013). However, similarly rapid changes occur during periods of low inflow rates (DOY 340 to DOY 365) so that thermocline movements are partly independent of river inflow. The temperature difference between bottom and surface layers is fairly small. For instance, a maximum observed temperature difference between $z = 10$ m and $z = 40$ m is $\Delta t = 2$°C so that the seiche period (T_{Seiche}) can be estimated using the common formation:

$$T_{Seiche} = \frac{2L}{\sqrt{g' z_{Th}}}$$

(e.g. Fischer *et al.* 1979) to be on the order of 36–48 h (with L being 10 km in Lake Ohau, g' is the reduced gravity due to temperature difference and $z_{Th} = \sim 20$ m is the depth of the thermocline). The amplitudes during this period are large (on the order of O(10) metres: Fig. 5*e*,*f*). Seiches with such amplitudes can cause velocities of 0.05–0.10 m s^{-1} and could be responsible for increased velocities during this period (Fischer *et al.* 1979).

Fig. 9*a* demonstrates the estimated depth of the thermocline and Fig. 9*b* shows the frequency and magnitude of thermocline excursions (Δz_{Th}). It is evident that ~40% of the time Δz_{Th} is larger than 5 m. Furthermore, the distribution is almost symmetrical, indicating that the thermocline is equally subjected to up- or downwelling and that a periodic motion in form of an internal wave is driven by a mechanism unrelated to river inflow.

Fig. 10 shows the Power Spectra Density of wind velocities and the estimated position of the thermocline. The dominant frequencies in the spectra (12- and 48-h intervals) compare favourably well. The offsets of the peaks could be attributed to the location of Site 3, which is not the downwind end but at the east end of the eastern basin (Fig. 1). Additionally, the thermocline was identified on the basis of four thermistor loggers over a depth of 50 m, which allows only for an estimate of the thermocline position in the water column. Nonetheless, Fig. 10 indicates that thermocline movements near the outflow can be linked with the wind-induced stress whereas the thermal regime near the inflow suggests that internal wave climate is greatly influenced by river inflow.

Conceptual model for seasonal changes in Lake Ohau

Lake Ohau is subjected to varying climate conditions and rainfall events manifested in strongly fluctuating river inflow rates that frequently trigger turbidity currents over an annual

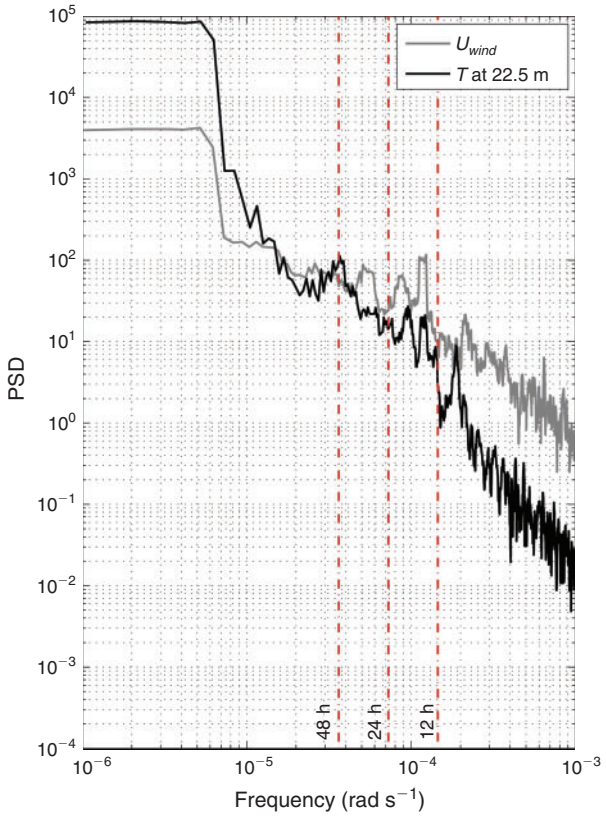

Fig. 10. Power spectra densities of the wind velocities at Killin Barn (grey) and the temperatures measured at $z = 22.5$ m near the outflow at Site 3 (black line). The vertical dashed lines depict 48-, 24- and 12-h periods.

cycle. The critical suspended sediment concentration required to trigger turbidity currents for freshwater lakes is fairly low at $\ll$1 kg m^{-3} (Mulder and Syvitski 1995). Although the sediment concentration of the inflow during floods is not known it can be easily concluded that the size of Lake Ohau's drainage area (~1200 km^2) and elevation (500–3000 m) produces average concentrations of at least 1 kg m^{-3} (Mulder and Syvitski 1995, fig. 7). It can be further concluded that floods flush the catchment area and river bed and yield even higher sediment concentrations at the head of the lake than during average discharge rates. Thus, on the basis of meteorological and hydrological forcing the sediment supply and deposition have to be differentiated into several stages representing different discharge rates and sediment concentration.

Fig. 11 presents a conceptual model of the observed processes that contribute to sedimentation and ultimately varve formation in Lake Ohau. In addition, Fig. 11 sketches further processes known from other lake studies that may add to the sedimentation regime but require further monitoring in Lake Ohau. Fig. 11*a* shows the conditions during Period 1, in which several flood events of $Q > 200$ m^3 s^{-1} were observed. Historically, inflows of this magnitude are relatively common and occur 6–7 times per year. Over our monitoring period these flows showed increased acoustic backscatter data and had warmer temperatures than the ambient fluid, indicating significant sediment concentration to overcome the buoyancy force. Owing to the density difference between inflow and lake the river waters propagate through the lake as underflows and reach the distal part of Lake Ohau, depositing fine (~5 μm) particles as measured in sediment traps by Roop *et al.* (2015) and also in accord with data obtained from LISST profiles (Fig. 4).

In addition, periodic cold water plumes (1°C colder than ambient water temperature) during regular inflow conditions were found to descend down the lake slope in the winter. Diurnal temperature fluctuations were still noticeable near the outflow with variations of up ~0.2°C (Roop *et al.* 2015) suggesting that these currents also reach the distal part of the lake or occur around the periphery of Lake Ohau. Cold water plumes could also develop from cold river inflow, which is cooled down by cold air temperatures at night. Though their origin is unclear, the driving force for periodic cold water bursts in Period 1 seems to be convectively driven density plumes that are an effective driver for flushing near-shore regions (e.g. Fer *et al.* 2002). The observed velocities associated with cold water plumes of 0.1 m s^{-1} are strong enough to erode and transport suspended sediment into more distal parts. Such density plumes could potentially contribute to the total annual sediment deposition in Lake Ohau but based on the low backscatter data they are less significant than sediment supplied by increased river discharge ($Q > 100$ m^3 s^{-1}) in Period 1.

Most sediment flux occurs during spring and summer and the corresponding thermal regime is depicted in Fig. 11*b* (moderate flood events with $Q \sim$ 100–500 m^3 s^{-1} reflect return periods of several times per year to 2 years) and Fig. 11*c* (large flood events with $Q > 500$ m^3 s^{-1}) respectively. Flood events of $Q > 500$ m^3 s^{-1} have a return period of ~2 years, implying that Lake Ohau receives greatly enhanced influxes of sediment several times a decade. The presence of steep temperature gradients during the summer is significant but its effect on the sedimentation regime remains speculative. The thermocline could act as a barrier to prevent finer particles from immediate settling. Rapid, periodic temperature fluctuations up to 5–6°C around the depth of 20 m near the outflow are either wind-induced or river-inflow-induced seiches that cause thermocline excursions near the outflow. However, breaking of internal waves could also cause sediment slumps and resuspension of particles leading to further sedimentation (Pharo and Carmack 1979). The internal wave climate is not entirely clear from this 1-year record. For instance, the presence of Kelvin waves associated with large bottom velocities, as observed in Lake Geneva (Lemmin *et al.* 2005), could be present but to detect such waves more thermistor chains around the periphery of Lake Ohau are required.

It is noteworthy that the 2012–13 summer season was relatively cold compared with other years and that flood events had a significant effect on the thermal variability of the lake. During warmer summers the thermal stratification would be much stronger, which puts more emphasis on the internal wave climate and related resuspension events in the wash-zone of the thermocline (Pharo and Carmack 1979; Peeters and Kipfer 2009). An additional source of sediment could stem from sediment resuspension caused by surface waves, as observed in Sunwapta Lake (Gilbert and Shaw 1981) and more recently in Lake Tahoe (Reardon *et al.* 2014). Generally, Lake Ohau has steep slopes and only small parts are shallow shelf areas, but due

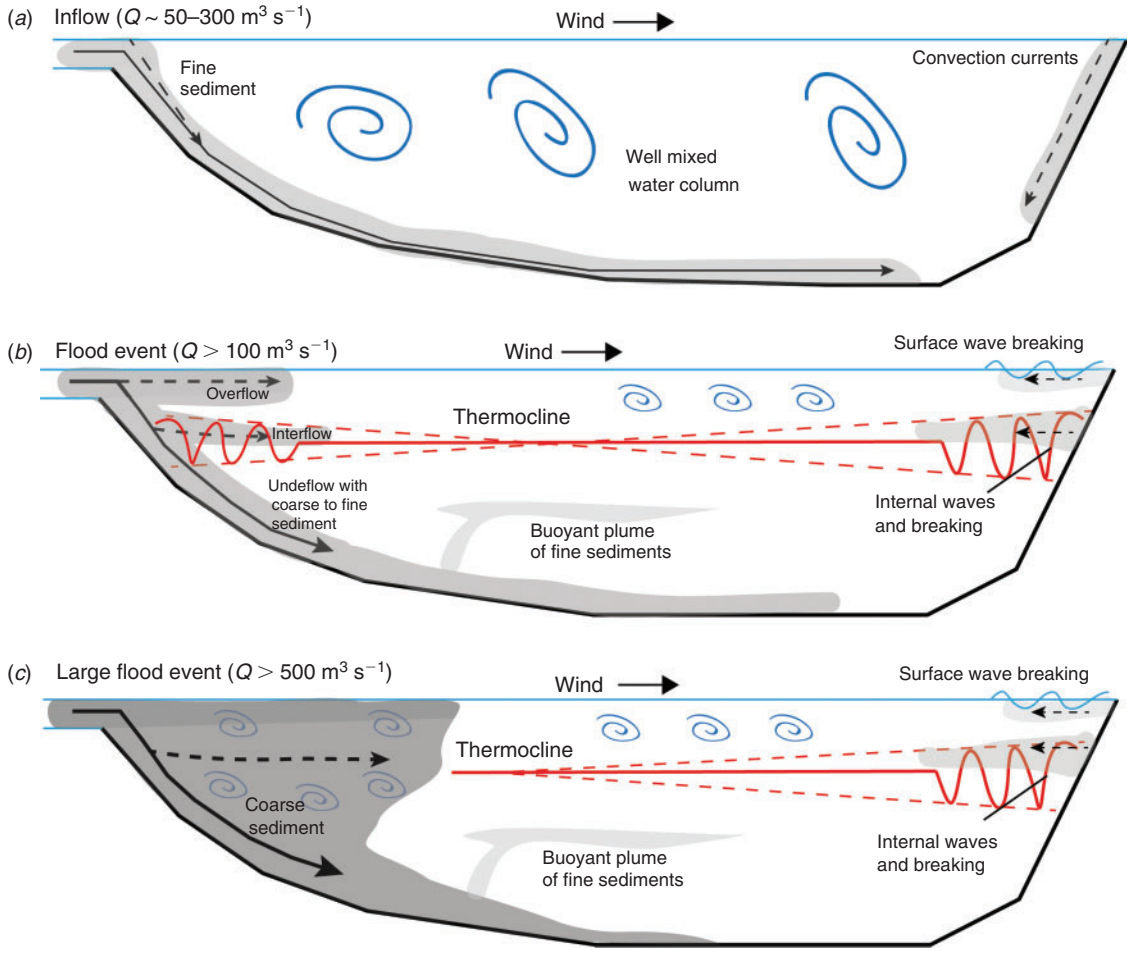

Fig. 11. Conceptual model of important processes in Lake Ohau in interannual sedimentation. (*a*) Winter period when the lake is isothermal; (*b*) summer period during flood events when the lake exhibits a strong thermal gradient; and (*c*) large flood event during Period 2 where the stratification is eroded near the inflow.

to the wind and wave climate along the north–south axis additional sediment could get resuspended near the south shore. For instance, this could explain the high sediment concentration near the bottom in the eastern basin depicted in Fig. 4*f*.

A strong thermal gradient also has an effect on river plumes and how they intrude in the lake system (Alavian *et al.* 1992). Inter- and overflows could play a bigger role during moderate floods, for instance when the thermocline is not eroded and a strong thermal gradient prevails or when inflows carry less sediment and are unable to pierce through the thermocline. This could cause the distribution of finer sediments across the lake (Fig. 11*b*), as seen in many other studies (e.g. Pharo and Carmack 1979; Lambert and Giovanoli 1988; Gilbert *et al.* 2006). Another mechanism that has been observed in several lakes is that underflows become buoyant after the coarse sediment has settled out of suspension and detach from the lake bed further away from the delta (Fig. 11*b*). This mechanism could also explain the presence of coarse sediment near the inflow and continuous fining of sediment towards the distal end of the lake.

On two occasions after heavy rainfall large floods with $Q > 900\ m^3\ s^{-1}$ triggered turbidity currents that reached heights of tens of metres and velocities of up to $0.4\ m\ s^{-1}$ in early 2013. Such large floods have return periods of 10 years. Near the inflow the thermal stratification is temporarily destroyed (Fig. 5*e*) but the lake still exhibits a thermal stratification at the outflow (Fig. 5*f*). Optical backscatter data (Fig. 6*f*) and turbidity measurements (NTU > 31) observed by Roop *et al.* (2015) and temperature inversions (Fig. 8*b*) indicate that the sediment load during these inflow events was very high. These flows produced large sediment fluxes into the lake with volumes of ~100 mm of lake bottom equivalent near the inflow and ~5 mm of lake bottom equivalent near the outflow (Roop *et al.* 2015). These values are comparable to maximum deposition rates in other intermontane lakes, for instance, in Kamloops Lake (Pharo and Carmack 1979) or in Lake Lillooet (Gilbert *et al.* 2006). Very large floods ($900–1000\ m^3\ s^{-1}$) occur at least once a decade in Lake Ohau and extreme flood events ($Q > 1500\ m^3\ s^{-1}$) have return periods of the order of 50 years. Thus, we hypothesise that distinctly thicker sediment layers associated with these events should be found near the delta and near the outflow on a decadal and centennial time scale. The sediment regime displays a strong seasonality and large floods cause the largest sediment input in late spring and summer when

most sediment is available from the catchment area. However, floods with $Q > 200$ m^3 s^{-1} occur several times throughout the year. Turbidity currents arise from these floods and operate mainly as underflows contributing to accumulation rates during the annual cycle.

Conclusions

Lake Ohau exhibits an extreme turbidity current regime with varying seasonal intensity. Sedimentation is mainly controlled by high sediment loads from river floods in the summer but these persist at lower frequency throughout the year. The processes sketched in Fig. 11 can occur independently, simultaneously, or even interact with each other, underlining the complexity of this lake system. To examine the interplay of these mechanisms on an interannual basis, a long-term monitoring program is required for Lake Ohau, ideally with a larger spatial and time-step resolution of thermistor chains near the inflow, at the downwind end of the lake and in the eastern basin. Moreover, ADCP instruments located further away from the inflow could provide information on whether bottom currents, inter- or surface flows dominate over the course of the year. The use of sediment traps, turbidity measurements at the inflow and monitoring of meteorological factors is in progress and will be required to understand the sedimentation regime. The development of numerical models is desirable to improve understanding of the system response to various conditions such as storms, rain events and floods. Field measurements, with the aim of understanding the importance of internal waves for sedimentation regime, characteristics of turbidity currents and sediment density surges at the delta will be the focus of future work in Lake Ohau and lead to a holistic model on varve formation.

Acknowledgements

This work was financially supported by the GNS Science 'Global Change through Time' program, the Sarah Beanland Memorial Scholarship, and the ANZICE program (VICX0704), PMEL Contribution Number 4122, and the Eggers fund. We thank Gary Wilson and the Marine Sciences Department, University of Otago, for logistical support. The National Science Foundation East Asia and Pacific Summer Institute supported Paul Stumpner. In addition, we thank Chris and Rae Spiers for their hospitality and large workspace at the Killin Barn, and the Inkersell family at Lake Ohau Station for land access and ongoing support. In addition, we thank three anonymous reviewers for their comments and suggestions, which helped to improve the manuscript.

References

Alavian, V., Gerhard, H., Jirka, R., Denton, A., Johnson, M. C., and Stefan, H. G. (1992). Density currents entering lakes and reservoirs. *Journal of Hydraulic Engineering* **118**, 1464–1489. doi:10.1061/(ASCE)0733-9429(1992)118:11(1464)

Amann, B., Mauchle, F., and Grosjean, M. (2014). Quantitative high-resolution warm season rainfall recorded in varved sediments of Lake Oeschinen, northern Swiss Alps: calibration and validation AD 1901–2008. *Journal of Paleolimnology* **51**, 375–391. doi:10.1007/S10933-013-9761-3

Baringer, M. O., and Price, J. F. (1997). Mixing and spreading of the Mediterranean outflow. *Journal of Physical Oceanography* **27**, 1654–1677. doi:10.1175/1520-0485(1997)027<1654:MASOTM>2.0.CO;2

Best, J. L., Kostaschuk, R. A., Peakall, J., Villard, P. V., and Franklin, M. (2005). Whole flow field dynamics and velocity pulsing within natural sediment-laden underflows. *Geology* **33**, 765–768. doi:10.1130/G21516.1

Cenedese, C., Whitehead, J. A., Ascarelli, T. A., and Ohiwa, M. (2004). A dense current flowing down a sloping bottom in a rotating fluid. *Journal of Physical Oceanography* **34**, 188–203. doi:10.1175/1520-0485(2004)034<0188:ADCFDA>2.0.CO;2

Chen, C. T., and Millero, F. J. (1986). Precise thermodynamic properties for natural waters covering only the limnological range. *Limnology and Oceanography* **31**, 657–662. doi:10.4319/LO.1986.31.3.0657

Dallimore, C. J., Imberger, J., and Ishikawa, T. (2001). Entrainment and turbulence in saline underflow in Lake Ogawara. *Journal of Hydraulic Engineering* **127**, 937–948. doi:10.1061/(ASCE)0733-9429(2001)127:11(937)

De Cesare, G., Boillat, J.-L., and Schleiss, A. J. (2006). Circulation in stratified lakes due to flood-induced turbidity currents. *Journal of Environmental Engineering* **132**, 1508–1517. doi:10.1061/(ASCE)0733-9372(2006)132:11(1508)

Desloges, J. R. (1994). Varve deposition and the sediment yield record at three small lakes of the southern Canadian Cordillera. *Arctic and Alpine Research* **26**, 130–140. doi:10.2307/1551776

Desloges, J. R., and Gilbert, R. (1994). Sediment source and hydroclimatic inferences from glacial lake sediments: the postglacial sedimentary record of Lillooet Lake, British Columbia. *Journal of Hydrology* **159**, 375–393. doi:10.1016/0022-1694(94)90268-2

Fer, I., Lemmin, U., and Thorpe, S. A. (2002). Contribution of entrainment and vertical plumes to the winter cascading of cold shelf waters in a deep lake. *Limnology and Oceanography* **47**, 576–580. doi:10.4319/LO.2002.47.2.0576

Fischer, H. B., List, E. J., Koh, R. C. Y., Imberger, J., and Brooks, N. H. (1979). 'Mixing in Inland and Coastal Waters.' (Academic Press: New York.)

Forrest, A. L., Laval, B. E., Pieters, R., and Lim, D. S. S. (2008). Convectively driven transport in temperate lakes *Limnology and Oceanography* **53**, 2321–2332. doi:10.4319/LO.2008.53.5_PART_2.2321

Gilbert, R. (1975). Sedimentation in Lillooet Lake, British Columbia. *Canadian Journal of Earth Sciences* **12**, 1697–1711. doi:10.1139/E75-151

Gilbert, R., and Butler, R. D. (2004). The physical limnology and sedimentology of Meziadin Lake, northern British Columbia, Canada. *Arctic, Antarctic, and Alpine Research* **36**, 33–41. doi:10.1657/1523-0430(2004)036[0033:TPLASO]2.0.CO;2

Gilbert, R., and Crookshanks, S. (2009). Sediment waves in a modern high-energy glacilacustrine environment. *Sedimentology* **56**, 645–659. doi:10.1111/J.1365-3091.2008.00990.X

Gilbert, R., and Shaw, J. (1981). Sedimentation in proglacial Sunwapta Lake, Alberta. *Canadian Journal of Earth Sciences* **18**, 81–93. doi:10.1139/E81-007

Gilbert, R., Crookshanks, S., Hodder, K. R., Spagnol, J., and Stull, R. B. (2006). The record of an extreme flood in the sediments of montane Lillooet Lake, British Columbia: implications for paleoenvironmental assessment. *Journal of Paleolimnology* **35**, 737–745. doi:10.1007/S10933-005-5152-8

Hamblin, P. F., and Carmack, C. (1978). River-induced currents in a fjord lake. *Journal of Geophysical Research* **83**, 885–899. doi:10.1029/JC083IC02P00885

Hardy, D. R. (1996). Climatic influences on streamflow and sediment flux into Lake C2, northern Ellesmere Island, Canada. *Journal of Paleolimnology* **16**, 133–149.

Jonas, T., Stips, A., Eugster, W., and Wüest, A. (2003). Observations of a quasi shear-free lacustrine convective boundary layer: stratification and its implications on turbulence. *Journal of Geophysical Research* **108**, 3328. doi:10.1029/2002JC001440

Kerr, T. (2013). The contribution of snowmelt to the rivers of the South Island, New Zealand. *Journal of Hydrology. New Zealand* **52**, 61–82.

Kim, Y. H., and Voulgaris, G. (2003). Estimation of suspended sediment concentration in estuarine environments using acoustic backscatter from an ADCP. In 'Proceedings of Coastal Sediments 2003: Crossing Disciplinary Boundaries', 18–23 May 2003, Clearwater, FL, USA. (Eds R. A. Davis, Asbury Sallenger, and P. Howd.) (CD-ROM) (World Scientific Publishing.)

Lambert, A. M., and Giovanoli, F. (1988). Records of riverborne turbidity currents and indications of slope failures in the Rhone delta of Lake Geneva. *Limnology and Oceanography* **33**, 458–468. doi:10.4319/LO.1988.33.3.0458

Leemann, A., and Niessen, F. (1994). Varve formation and the climatic record in an alpine proglacial lake; calibrating annually-laminated sediments against hydrological and meteorological data. *The Holocene* **4**, 1–8. doi:10.1177/095968369400400101

Lemmin, U., Mortimer, C. H., and Bäuerle, E. (2005). Internal seiche dynamics in Lake Geneva. *Limnology and Oceanography* **50**, 207–216. doi:10.4319/LO.2005.50.1.0207

Middleton, G. V. (1993). Sediment deposition from turbidity currents. *Annual Review of Earth and Planetary Sciences* **21**, 89–114. doi:10.1146/ANNUREV.EA.21.050193.000513

Mulder, T., and Syvitski, J. P. M. (1995). Turbidity currents generated at river mouths during exceptional discharges to the world oceans. *The Journal of Geology* **103**, 285–299. doi:10.1086/629747

Ojala, A. E. K., Francus, P., Zolitschka, B., Besonen, M., and Lamoureux, S. F. (2012). Characteristics of sedimentary varve chronologies: a review. *Quaternary Science Reviews* **43**, 45–60. doi:10.1016/J.QUASCIREV.2012.04.006

Patterson, J. C., Hamblinet, P. F., and Imberger, J. (1984). Classification and dynamic simulation of the vertical density structure of lakes. *Limnology and Oceanography* **29**, 845–861. doi:10.4319/LO.1984.29.4.0845

Peeters, F., and Kipfer, R. (2009). Currents in stratified water bodies 1: density-driven flows. In 'Encyclopedia of Inland Waters'. (Ed. G. E. Likens.) Vol. 1, pp. 530–538. (Academic Press: London.)

Pharo, C. H., and Carmack, E. C. (1979). Sedimentation processes in a short residence-time intermontane lake, Kamloops Lake, British Columbia. *Sedimentology* **26**, 523–541. doi:10.1111/J.1365-3091.1979.TB00927.X

Putnam, A. E., Schaefer, J. M., Denton, G. H., Barrell, D. J., Birkel, S. D., Andersen, B. G., Kaplan, M. R., Finkel, R. C., Schwartz, R., and Doughty, A. M. (2013). The Last Glacial Maximum at 44°S documented by a 10Be moraine chronology at Lake Ohau, southern Alps of New Zealand. *Quaternary Science Reviews* **62**, 114–141. doi:10.1016/J.QUASCIREV.2012.10.034

Reardon, K. E., Bombardelli, F. A., Moreno-Casas, P. A., Rueda, F. J., and Schladow, S. G. (2014). Wind-driven nearshore sediment resuspension in a deep lake during winter. *Water Resources Research* **50**, 8826–8844. doi:10.1002/2014WR015396

Roop, H. A., Dunbar, G. B., Levy, R., Vandergoes, M. J., Forrest, A. L., Walker, S. L., Purdie, J., Upton, P., and Whinney, J. (2015). Seasonal controls on sediment transport and deposition in Lake Ohau, South Island, New Zealand: implications for a high-resolution Holocene palaeoclimate reconstruction. *Sedimentology* **62**, 826–844. doi:10.1111/SED.12162

Thompson, D. W. J., and Solomon, S. (2002). Interpretation of recent Southern Hemisphere climate change. *Science* **296**, 895–899. doi:10.1126/SCIENCE.1069270

Thorpe, S. A., Lemmin, U., Perrinjaquet, C., and Fer, I. (1999). Observations of the thermal structure of a lake using a submarine. *Limnology and Oceanography* **44**, 1575–1582. doi:10.4319/LO.1999.44.6.1575

Tylmann, W., Szpakowska, K., Ohlendorf, C., Woszczyk, M., and Zolitschka, B. (2012). Conditions for deposition of annually laminated sediments in small meromictic lakes: a case study of Lake Suminko (northern Poland). *Journal of Paleolimnology* **47**, 55–70. doi:10.1007/S10933-011-9548-3

Ummenhofer, C. C., Gupta, S., and England, M. H. (2009). Causes of late twentieth-century trends in New Zealand precipitation. *Journal of Climate* **22**, 3–19. doi:10.1175/2008JCLI2323.1

Weirich, F. (1986). The record of density-induced underflows in a glacial lake. *Sedimentology* **33**, 261–277. doi:10.1111/J.1365-3091.1986.TB00535.X

Wells, M. G., Cenedese, C., and Caulfield, C. P. (2010). The relationship between flux coefficient and entrainment ratio in density currents. *Journal of Physical Oceanography* **40**, 2713–2727. doi:10.1175/2010JPO4225.1

Woods, R., Hendrikx, J., Henderson, R., and Tait, A. (2006). Estimating mean flow of New Zealand rivers. *Journal of Hydrology. New Zealand* **45**, 95–110.

Wunderlich, W. O. (1972). Heat and mass transfer between a water surface and the atmosphere. Division of Water Resources Research, Report 14, Tennessee Valley Authority, Norris, TN.